Chem Soc Rev

RSC Publishing

TUTORIAL REVIEW

Mesoporous materials for antihydrogen production†

Cite this: *Chem. Soc. Rev.*, 2013, **42**, 3821

Giovanni Consolati,*[ab] Rafael Ferragut,[bc] Anne Galarneau,[d] Francesco Di Renzo[d] and Fiorenza Quasso[a]

Antimatter is barely known by the chemist community and this article has the vocation to explain how antimatter, in particular antihydrogen, can be obtained, as well as to show how mesoporous materials could be used as a further improvement for the production of antimatter at very low temperatures (below 1 K). The first experiments with mesoporous materials highlighted in this review show very promising and exciting results. Mesoporous materials such as mesoporous silicon, mesoporous material films, pellets of MCM-41 and silica aerogel show remarkable features for antihydrogen formation. Yet, the characteristics for the best future mesoporous materials (*e.g.* pore sizes, pore connectivity, shape, surface chemistry) remain to be clearly identified. For now among the best candidates are pellets of MCM-41 and aerogel with pore sizes between 10 and 30 nm, possessing hydrophobic patches on their surface to avoid ice formation at low temperature. From a fundamental standpoint, antimatter experiments could help to shed light on open issues, such as the apparent asymmetry between matter and antimatter in our universe and the gravitational behaviour of antimatter. To this purpose, basic studies on antimatter are necessary and a convenient production of antimatter is required. It is exactly where mesoporous materials could be very useful.

Received 7th November 2012

DOI: 10.1039/c2cs35454c

www.rsc.org/csr

Key learning points

- Chemical and physical features of mesoporous materials (in particular, MCM-41 and aerogels) are particularly suitable to generate antimatter at low energy, the only one chance to study the properties of antimatter.
- A new challenging way to generate antihydrogen from positronium atoms, which are efficiently produced by means of positrons interacting with mesoporous silica.
- Properties of positronium, the lightest element of the universe; methods to detect it; effects of its interactions with mesoporous materials.
- Importance of antimatter: to understand fundamental laws of nature as gravitation and for current and future uses, in particular as a possible source of energy.

1. Introduction

For many people antimatter is a topic belonging to science fiction, made famous by the Dan Brown's best seller *Angels & Demons* or by the T.V. series Star Trek. Yet, antimatter not only exists but an important medical technology is based on it: the positron emission tomography (PET), an imaging technique able to supply a three-dimensional picture of functional processes in the body.[1] According to the current view in physics, with each particle is associated an antiparticle with identical mass but opposite charge. The most striking feature of antimatter is the annihilation process. Indeed, when a particle–antiparticle pair collides the mass of the system is converted into electromagnetic energy, in the case of electron–positron pairs, or in other lighter particles for heavier particles such as the proton–antiproton pair. Just the detection of the gamma rays emitted from the electron–positron annihilation makes possible in the PET the reconstruction of the position of the tracer emitting positrons in the body of the patient, by allowing the location of metastases or the diagnosis of brain diseases. Still in the medical field, although proton radiotherapy is a rapidly advancing field, antiprotons are proposed as a valid alternative, due to a more precise and efficient energy deposition at the end of their range.[2] Furthermore, annihilation occurring when antiprotons stop would offer the unique advantage to monitor in real time the process. Antimatter also supplies a tool for materials science studies, by exploiting the annihilation features in

[a] *Department of Aerospace Science and Technology, Politecnico di Milano, via La Masa 34, 20156, Milano, Italy. E-mail: giovanni.consolati@polimi.it, fiorenza.quasso@polimi.it; Fax: +39 2 23998334; Tel: +39 2 23998353*

[b] *Istituto Nazionale di Fisica Nucleare, via Celoria 16, 20133 Milano, Italy*

[c] *LNESS and CNISM, Dipartimento di Fisica, Politecnico di Milano, Via Anzani 42, 22100, Como, Italy. E-mail: rafael.ferragut@polimi.it; Fax: +39 0313327617; Tel: +39 0313327338*

[d] *Institut Charles Gerhardt Montpellier, UMR 5253 CNRS-UM2-ENSCM-UM1, ENSCM, 8 Rue Ecole Normale, 34296, Montpellier, France. E-mail: anne.galarneau@enscm.fr, francesco.di-renzo@enscm.fr; Fax: +33 4 67 16 34 70; Tel: +33 4 67 16 34 68*

† Part of the mesoporous materials themed issue.

condensed matter. Indeed, positrons entering into a medium annihilate with the surrounding electrons and disappear with time, according to an exponential decay. Lifetime of positrons depends on the local electron density of the medium: it increases in the presence of a defect, characterized by a lower electron density with respect to the bulk. Therefore, the positron is a useful probe to investigate subnanometric defects in solids, such as vacancies in metals[3] or defects in semiconductors,[4] as well as to follow structural transformations those materials undergo. Sensitivity is very high in a metal, ppm concentrations are sufficient to produce a clearly detectable signal. It is possible to obtain not only the density of the defects but also their size, their spatial distribution and information on the chemical nature of the environment. Positron annihilation techniques are currently used also to investigate the free volume in polymers,[5] to study hybrid solar cells[6] or to characterize porous inorganic structures,[7] with various advantages: they are nondestructive tools and the spatial resolution is not limited to a single plane. Pore sizes from a few tenths to several tens of nm can be detected and their size distribution estimated. Both interconnected and buried, isolated pores, not accessible to conventional probes, can be revealed.

Other practical uses of antimatter probably do not belong to the immediate future. Present production of antimatter is scanty: antiparticles are generated only in laboratories using suitable radioactive sources or accelerators; just more complex structures such as antihydrogen are produced only at CERN in very tiny amounts. However, astonishing numbers of antiparticles are expected to be produced in the future by extremely high intensity lasers.[8] Antimatter has been proposed to fuel engines: indeed, the energy per unit mass released by annihilation is about 10 orders of magnitude higher than a typical chemical reaction. It is true that antimatter cannot be stored in a conventional vessel, since annihilation would take place with the walls of the container. However, antimatter can be confined into traps (Penning traps) formed by electric and magnetic fields.

Another challenging development of antimatter is to use positronium (Ps), the bound state of an electron and a positron, to build a gamma-ray laser.[9] Ps, the lightest element (about 10^{-3} times lighter than hydrogen), exists in the ground state in two sublevels: singlet (*para*-Ps, *p*-Ps) and triplet (*ortho*-Ps, *o*-Ps), according to the spins of the electron and positron (antiparallel or parallel, respectively). In a vacuum their lifetimes are very different, equal to 0.125 and 142 ns for *p*-Ps and *o*-Ps, respectively.

From left to right: Giovanni Consolati, Rafael Ferragut, Anne Galarneau, Francesco Di Renzo and Fiorenza Quasso

Giovanni Consolati was born in Milano, Italy, in 1956 *and obtained degrees in Nuclear Engineering and in Physics. He has been an Associate Professor in Physics at the Politecnico di Milano since* 1999. *His research activity focused on: hyperfine splitting of positronium and its chemical reactions with condensed matter; interactions between polarized positrons and organic media, with the discovery of positron spin relaxation phenomena; studies of porosities in clays, cements and of the free volume in polymers, with the proposal of a model of an anisotropic increase of free volume holes. He collaborates at CERN to produce antihydrogen for gravity experiments on antimatter.*

Rafael Ferragut was born in Buenos Aires, Argentina, and has been an Assistant Professor in the Department of Physics at Politecnico di Milano since 2005. *He received his PhD in Physics in* 1999 *from Universidad Nacional del Centro de la Provincia de Buenos Aires. Rafael's current research focuses on applied studies in Materials Science and Antimatter properties. He studies porous materials, thin films (hybrid solar cells, semiconductors, oxides, etc.) and age-hardenable alloys. He has been responsible of the Positron Laboratory at the research centre L-NESS in Como since* 2010. *He collaborates with the antimatter experiment AEgIS that takes place at CERN.*

Dr Anne Galarneau was born in Les Sables d'Olonne, France, in 1967 *and obtained her PhD ès Science in* 1993 *from the University of Nantes, France. She joined the group of Prof. T. Pinnavaia at the University of Michigan, USA, and then settled at Montpellier as a CNRS researcher in* 1995. *Her research interests include the synthesis of mesoporous silica and their applications in biocatalysis, catalysis and adsorption. Her main discoveries concern the pseudomorphic transformation for morphology control, the phospholipid-templated silica for enzymes encapsulation, the SBA-15 structure resolution, the meso-macroporous monoliths for catalysis in flow, the zeolite monoliths for wastewater treatment.*

Francesco Di Renzo obtained chemical engineering degree and PhD in industrial chemistry (Politecnico di Milano), and is the research director at CNRS, head of the MACS team (Advanced Materials for Catalysis and Healthcare) of the ICGM (Institut Charles Gerhardt Montpellier). He started his research activity on the heterogeneous catalysis of mild oxidation reactions and later developed methods for the synthesis and the textural control of porous catalysts and adsorbents. Actually he is involved in the development of catalytic processes for the valorisation of renewable resources. He was the past president of the GFZ (French Zeolite Group) and the past secretary of the IZA (International Zeolite Association).

Fiorenza Quasso graduated in Physics in 1983 *at the Università di Milano; in* 1989 *she obtained her PhD in Physics at the Politecnico di Milano. She became an Associate Professor in Experimental Physics in* 2006. *Her research activity is addressed to the experimental study of thermal properties of polymeric materials by means of differential scanning calorimetry. Furthermore, she investigates the free volume of polymers and nanometric cavities in porous materials by means of Positron Annihilation Spectroscopies.*

Also annihilation features in a vacuum are different: *p*-Ps annihilates with emission of two gamma rays, while *o*-Ps annihilates by emitting three gamma rays. A high density of Ps could be achieved by accumulating a sufficient amount of low energy positrons in a trap, then sending them focused to a small spot on a Ps-forming mesoporous target. Starting annihilation on the collection of Ps atoms would give rise to stimulated emission of gamma radiation. The number of accumulated positrons up to the present (about 10^8) is too low to produce the required amount of Ps atoms (at least 10^{15}), but enormous progress was made in the last few years in positrons confinement. Therefore, the objective of an antimatter-driven laser is realistic, although not immediate.

The only antiatom, which will be probably investigated in the near future is the simplest one, that is, antihydrogen ($\bar{H}$), formed by a positron orbiting around a nucleus made up of an antiproton. $\bar{H}$ is fundamental to test the gravitational interaction of antimatter. Although matter and antimatter are expected to have identical gravitational properties, the problem is still under debate[10] and until now it has not been possible to carry out experiments. Matter and antimatter could repel each other, in spite of being self-attractive.[11] The interest for this subject is supported by the recent finding[12] of the accelerated expansion of the universe (the Nobel Prize for Physics was assigned in 2011 for this topic), which could be explained by some kind of gravitational repulsion, as an alternative hypothesis of the dark matter and dark energy.

Four experiments: ALPHA (Antihydrogen Laser PHysics Apparatus), ATRAP (Antihydrogen TRAP), ASACUSA (Atomic Spectroscopy And Collisions Using Slow Antiprotons) and AEgIS (Antihydrogen Experiment: gravity, Interferometry, Spectroscopy) are running at CERN in order to produce antihydrogen. In particular, the AEgIS experiment, which aims to measure the gravitational acceleration on $\bar{H}$, requires an intermediate step to generate Ps. Since Ps is produced from positrons impinging a suitable target, the choice of the positron converter is crucial for the success of the antihydrogen experiment. This review highlights the fact that mesoporous materials such as MCM-41-type and aerogels are until now among the best candidates as positron converters able to produce Ps with the required features to carry out such gravity measurements.

Therefore, after a short introduction to the AEgIS experiment and to the techniques able to detect Ps, we will discuss the investigations performed until now on various mesoporous materials, which are promising to explore antimatter production.

2. AEgIS experiment to produce antihydrogen

The first goal of the AEgIS collaboration[13] is to produce an antihydrogen beam from the reaction between Ps issued from mesoporous materials (Ps converter in Fig. 1 and 2) and antiprotons. Antiprotons $\bar{p}$ confined in a Penning trap are cooled down to temperatures of the order of 0.1 K; then, they interact with Ps previously excited in a Rydberg state

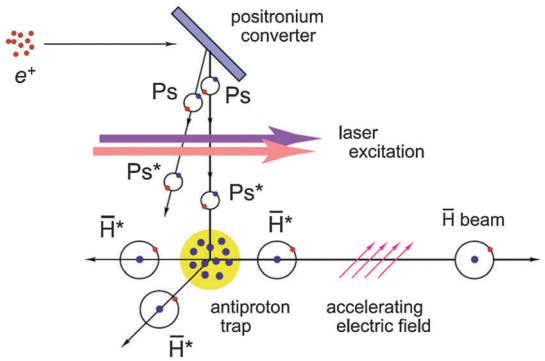

Fig. 1 Antihydrogen generation and subsequent acceleration in the AEgIS experiment (reprinted figure with permission from ref. 13. Copyright (2008) by Elsevier B.V. DOI: 10.1016/j.nimb.2007.12.010).

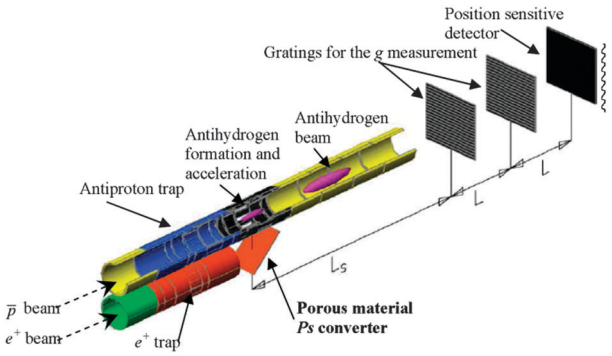

Fig. 2 Sketch of the AEgIS experiment for the measurement of the antihydrogen gravitational acceleration (reprinted figure with permission from ref. 14. Copyright (2010) by IOP Publishing Ltd. DOI: 10.1088/1742-6596/225/1/012007).

(Ps*, which is characterized by high values of the principal quantum number n, with $20 \leq n \leq 35$) by means of two laser pulses:

$$o\text{-Ps}^* + \bar{p} \rightarrow \bar{H}^* + e^- \quad (1)$$

For antimatter experiments only Ps in the triplet state (*o*-Ps) is interesting, since the lifetime of *p*-Ps is too short to allow the reaction (1) before annihilation. Eqn (1) represents a charge exchange reaction. Antihydrogen will also be formed in a Rydberg state, $\bar{H}^*$, at an average temperature of about 0.1 K, which corresponds to a mean velocity of the order of 50 m s^{-1}. Since the electric dipole moment of a Rydberg atom increases with n^2, $\bar{H}$ will be extracted from the environment where it is produced by using a force proportional to the $\bar{H}$ dipole moment and to an electric field gradient (Stark acceleration technique). A sketch of the process is shown in Fig. 1. Antihydrogen will be accelerated by producing a pulsed $\bar{H}$ beam, needed for gravity measurements. The beam, on passing between two identical gratings, will generate an interference pattern, registered on a plane parallel to the two gratings by means of suitable detectors. Owing to the gravitational force, the interference pattern will be vertically displaced by a distance:

$$\delta x = -gT^2, \quad (2)$$

where $T = L/v$ is the time of flight between each pair of gratings for a particle moving with speed v; L is the distance between consecutive gratings. Acceleration gravity g will be obtained from the measurement of the quantities T and δx. A schematic drawing of the whole apparatus is shown in Fig. 2.

Use of *o*-Ps excited in a Rydberg state would be useful not only to extract the antiatoms, but also because the cross section of the reaction (1) increases approximately as n^4, provided that the velocity of the Ps centre of mass is comparable to the velocity of the internal motion of the positron, averaged along its orbit. Since this last velocity is proportional to $1/n$, as it is obtained by using the simple Bohr model, it is low for a Rydberg *o*-Ps atom. The consequence is that the reaction (1) occurs with high probability only if Ps has low velocity, that is, low kinetic energy. In other words, Ps must be sufficiently 'cold'. Obviously, a high *o*-Ps yield increases the rate of the reaction (1). Therefore, a fundamental condition for the success of the gravitational experiment on $\bar{H}$ is the abundant production of cold *o*-Ps. It is essential to have a mesoporous material allowing us to obtain *o*-Ps with the required features, by starting from the positrons. The last, produced by a ^{22}Na radioactive source, are slowed down using a solid Ne moderator and trapped into an accumulator, where they lose energy through collisions with a gas (nitrogen) at suitable pressure. About 10^8 positrons in 300 s are stored. Then, a positrons bunch will be accelerated to energies of a few keV and implanted on a suitable target (mesoporous material), which will convert positrons into Ps. Since the characterization of a converter for *o*-Ps production is carried out by using various techniques based on positron annihilation, it is convenient to briefly discuss them before showing the main properties of the mesoporous material converters investigated until now.

3. Basis of Ps detection

Even if not broadly used by the material chemists, positron annihilation lifetime spectroscopy and Ps time of flight measurements are useful tools to characterize the porosity of materials (pore size, pore tortuosity and interconnectivity).

A positron injected into a medium loses its energy through inelastic collisions with the surrounding medium and reaches thermal energies within a negligible time interval (few ps). Positrons are generally obtained from the ^{22}Na radioisotope, which also emits within 3 ps a γ-ray with an energy of 1.274 MeV. This start signal marks the birth of the positron. The stop signal is supplied by one of the annihilation photons.

A schematic diagram of a positron annihilation lifetime spectrometer is shown in Fig. 3. It is formed by two detector channels: each consisting of a scintillator coupled to a photomultiplier tube (PMT). The scintillator converts the start or stop γ-ray into UV and visible photons which are absorbed by the window of the PMT, producing the emission of photoelectrons. They are multiplied by a series of intermediate dynodes; the resulting voltage is proportional to the energy of the γ-ray emitted by the scintillator. A constant fraction discriminator (CFD) on each channel distinguishes between start and stop

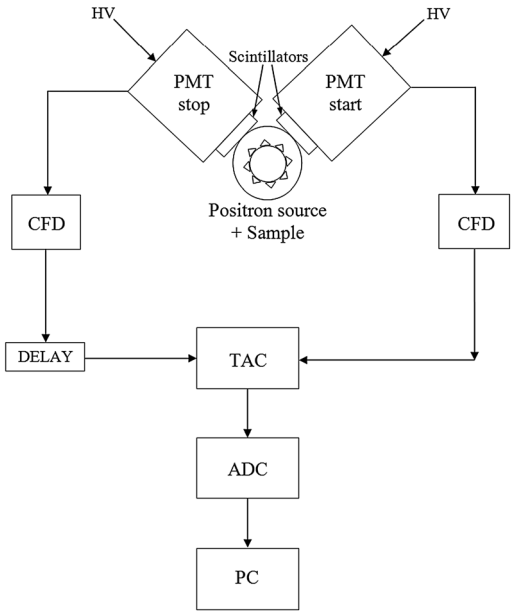

Fig. 3 Sketch of a typical positron annihilation lifetime spectrometer.

events on the basis of the different energies of the detected γ-ray. A time-to-amplitude converter (TAC) enabled by the start signal produces a voltage proportional to the time interval elapsed between generation and annihilation of the positron. This signal is digitized by an analog-to-digital converter (ADC) and transferred to the memory of a personal computer (PC).

The annihilation lifetime spectrum assumes the form of an histogram, which can be analyzed by means of a computer program in terms of the sum of a number of components; each one is an exponential function of the form $(I/\tau)\ \exp(-t/\tau)$, characterized by a lifetime τ and an intensity I. Analyses in terms of three components are quite common, but porous materials generally require a fourth component. *o*-Ps shows the longest lifetimes.

Positrons coming from ^{22}Na are very fast (kinetic energy up to 545 keV) and are implanted up to hundreds of microns into the sample: the probability of Ps emission from the surface into the vacuum is practically null. The remedy is to use a monoenergetic beam, tunable from about 50 eV up to 20 keV. This allows one to selectively explore subsurface layers from a few tens of nanometres up to some micrometers (depending on the maximum implantation energy of the beam and the density of the studied material).

There are two types of positron beams, continuous and pulsed. A continuous positron beam is basically composed of the following parts: (a) positron source; (b) moderator (typically a W foil or solid Ne), where a small fraction (less than 10^{-2}) of the positrons thermalize and are emitted with an energy of about 1 eV; (c) magnetic or electrostatic optics for transport of fixed energy (about 1–2 keV); (d) energy filtering to suppress the high energy background; (e) optics for accelerating, energy tuning and final focusing on the target. The voltage between the source and the target determines the energy of the incident positrons. The apparatus must be kept under ultra high vacuum

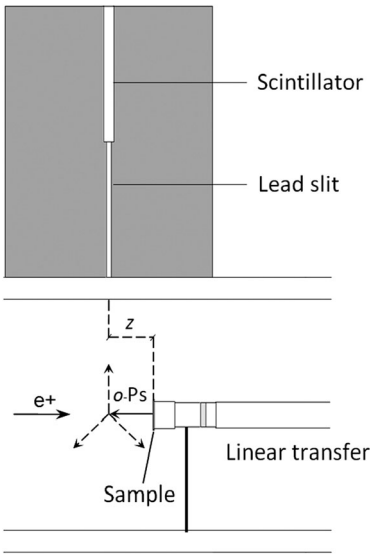

Fig. 4 Schematic diagram of the Ps-TOF apparatus. The positron beam comes from the left hand side and it is implanted into the sample. *o*-Ps is formed on the porous surface and/or into the bulk of the sample material and then it is emitted outside. The scintillator detects the γ-rays coming from the annihilated *o*-Ps. It is thus possible to obtain the kinetic energy distribution of the *o*-Ps atom into the vacuum.

to avoid loss of positrons annihilating with the gas molecules. The sample is viewed through a thin foil window using one (or more) Ge detector for Doppler broadening measurements.

The measurements with pulsed beams are normally associated with experiments where many positrons are involved.[15] Positron trapping and accumulation[16] makes possible experiments with pulsed bunches at high density of particles. Positron lifetime and Ps time of flight measurements are possible with the use of a pulsed beam with a well defined start signal. The necessary positrons to form Ps and produce cold antihydrogen for the AEgIS experiment are generated by means of a pulsed beam.

Positronium time of flight spectroscopy (Ps-TOF) is another effective technique for porous material research. It is particularly suitable to analyze the porosity, pore tortuosity and the velocity distribution of *o*-Ps outside the studied material. Ps-TOF is useful to check *o*-Ps cooling through collisions with the inner walls of porous material. A schematic diagram of the Ps-TOF apparatus is presented in Fig. 4. The sample is bombarded by a slow positron beam. Positrons are implanted into the appropriate porous sample and form *o*-Ps at the porous surface and/or inside the bulk.[17] In the case of interconnected pores open at the surface *o*-Ps can diffuse out of the film and can be detected using the Ps-TOF spectrometer. The time interval between the positron arrival to the sample to form Ps (start signal) and the detection of the gamma ray from the emitted *o*-Ps self-annihilation outside the sample in front to the lead slit at a distance z (stop signal – Fig. 4) is measured. It is thus possible to obtain the Ps-TOF spectra for an incident Ps kinetic energy. Knowing the distance z between the sample surface and the slit, the kinetic energy distribution of the emitted *o*-Ps can be obtained.[18]

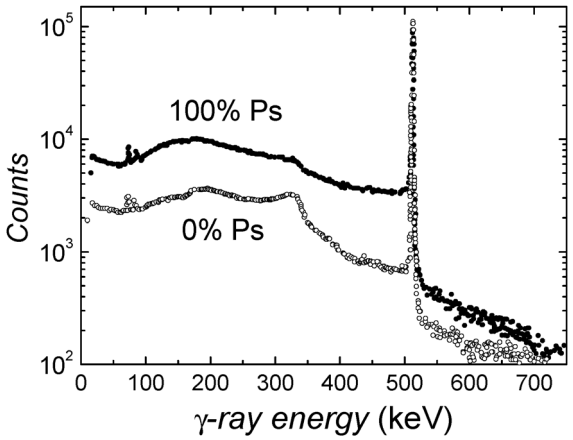

Fig. 5 Annihilation γ-spectra measured using a Ge detector at an Al(110) surface, where no positronium is formed (0% Ps) and where 100% Ps emission occurs at 900 K. Both curves were normalized to an equal height of the 511 keV line. (reprinted figure with permission from ref. 20. Copyright (1986) by Elsevier B.V.).

Measurement of Ps formation yield can be performed by means of a monoenergetic positron beam using the "3γ method".[19] This method is based on the idea that free positrons and *p*-Ps annihilate with emission of two gamma rays of 511 keV, while *o*-Ps annihilates by emitting three gamma rays producing a continuous energy distribution between 0 and 511 keV, where the sum of the energy of the three photons is 1022 keV. A Ge detector is normally used to collect the annihilation γ spectrum. From the annihilation spectrum it is possible to obtain the $R(E)$ parameter:

$$R(E) = \frac{V}{P} \tag{3}$$

where P and V are the integrated counts (after background subtraction) in the peak (511 ± 4.25 keV) and the "valley" area (from 350 keV up to 500 keV) that is a portion of the three gamma energy distribution of *o*-Ps annihilation (an example is given in Fig. 5). When Ps is emitted into vacuum, the positronium fraction $f(E)$ can be obtained from $R(E)$ using the relationship:[19]

$$f(E) = \left[1 + \frac{P_1(R_1 - R(E))}{P_0(R(E) - R_0)}\right]^{-1} \tag{4}$$

where P_0 and R_0 are the parameters when the positronium fraction is nil ($f = 0$) and P_1 and R_1 are the parameters when 100% of the positrons form Ps ($f = 1$). When Ps is formed inside the pores, the pick-off effect (the positron annihilates with an electron of the material, rather than the *o*-Ps electron, in a relative singlet state and two γ-rays – instead of three γ-rays – are emitted[21]) reduces the probability of 3γ annihilations by a factor:

$$\varepsilon = \frac{\lambda_{3\gamma}}{\lambda_{3\gamma} + \lambda_{\text{p.o.}}} \tag{5}$$

where $\lambda_{3\gamma} = (142\ \text{ns})^{-1}$ is the 3γ annihilation rate into vacuum and $\lambda_{\text{p.o.}}$ the pick-off annihilation rate. Thus the proper expression for the Ps fraction becomes:

$$F(E) = \varepsilon^{-1} f(E) \tag{6}$$

The factor ε^{-1} can be evaluated for high positron implantation energies from the available lifetime measurements. In all other cases the result obtained from eqn (4) is reported as "3γ fraction" ($f_{3\gamma} = f$). The "3γ fraction" is a useful parameter to assess the potential of a material to emit Ps that has lost kinetic energy by collisions while meandering through open pores.

The calibration for 0% and ~100% of Ps into the vacuum can be performed by using a Ge single crystal (100) or a metal (Fig. 5).[20] R_1 is obtained by extrapolation to zero implantation energy of the $R(E)$ curve measured in the sample at 1000 K (in this case 100% Ps formation occurs);[19] R_0 is the value of $R(E)$ at the highest positron implantation energy (0% Ps formation).

4. Porous materials for Ps production

4.1 Ps formation and cooling

Ps can be formed in metals and semiconductors only at the surface, when a thermalized positron captures an electron:[15] the high electronic density of these materials makes impossible Ps formation inside the homogeneous material. In contrast, Ps formation is possible in the bulk of an insulator; Ps formed can rise again at the surface and be emitted outside the material.

According to the Heisenberg principle, the minimum energy of Ps confined in a void with diameter d is $E = h^2/4md^2$, where h is the Planck constant and m is the Ps mass. Therefore, Ps cannot thermalize at room temperature if $d < 3$ nm. This excludes to use polymeric materials as Ps converters: besides practical difficulties to keep them into the vacuum at cryogenic temperatures (fragility, outgassing), the biggest pore diameters in poly[1-(trimethyl-silyl)propine], one of the polymers with the highest permeability, are less than 2 nm at room temperatures,[22] and shrinking is expected at lower temperatures.

On the other hand, in porous insulators Ps can be emitted in the internal porosities. If the pores have nanometric sizes *o*-Ps lifetime is reduced with respect to its value in a vacuum due to the pick-off process.[21] If the pores are interconnected Ps will diffuse between different pores and if the interconnections extend to the target surface a fraction of Ps may be emitted into the vacuum.[23]

Ps formation is documented in several porous materials.[6,14,24,25] The size of the pores is an important factor to obtain a suitable *o*-Ps cooling. Indeed, the minimum kinetic energy (or, equivalently, the minimum temperature) which *o*-Ps attains in the pore through the energy loss by a collisional mechanism with the walls depends on the size of the pore itself. By increasing the transverse size of the pore the temperature decreases and could reach values below 10 K for diameters higher than 20 nm. Of course, a compromise is necessary since the thermalization time of *o*-Ps increases with the size of the channel.

Mesoporous materials based on silica are extensively investigated, since a high fraction of the implanted positrons form *o*-Ps,[15] which can be emitted in the pore with a kinetic energy of 1–3 eV.[17] *o*-Ps loses its kinetic energy and cools down by means of collisions with the walls of the pore. We have seen (Section 2) that it is fundamental to produce *o*-Ps as cold as possible; however, only few papers report studies on Ps formation below room temperature. Mariazzi *et al.*[26] show that by implanting positrons at 7 keV in the target held at 150 K, about 27% of positrons form Ps that escapes into the vacuum. Besides, by means of Ps-TOF measurements, the authors estimate that around 9% of the escaped Ps (*i.e.* 2.6% of the implanted positrons) is cooled by collisions with the walls of mesopores and is emitted as a maxwellian beam at 150 K. *o*-Ps at temperatures below 150 K was emitted by an Al surface covered by a few oxygen monolayers;[27] unfortunately, the need of a careful control of the growing conditions as well as the sensitivity of oxygen to the temperature of the sample make this system not useful as a low temperature converter.

Time-of-flight measurements of Ps (Ps-TOF) emitted into the vacuum from porous films with interconnected porosities open towards the vacuum have given evidence of partial thermalization of Ps also at low temperatures in porous silica.[28]

As previously mentioned, the tortuosity of the pores influences the Ps slowing down in materials,[18] but also the chemical nature of the walls has an effect.[29] For instance, mesoporous silica films of SBA-15 type materials synthesized from the same triblock copolymer surfactant, but with different silane and/or methylsilane as a silica source featuring different surface chemistry (–H/–OH, $–CH_3$, –OH and $–CH_3$/–OH)[30] showed in Ps-TOF spectra a more effective Ps slowing down in the materials possessing –H/–OH surface groups only. Methyl groups at the surface helped to maintain a higher speed of Ps and a higher energy. The same observation was done for methyl-silsesquioxane (MSSQ) in comparison to hydrogen-silsesquioxane (HSSQ);[31] Ps-TOF measurements showed a lower *o*-Ps energy emitted out of the materials for HSSQ. However in this case, it is not easy to conclude about the effect of surface chemistry as HSSQ is a material with a higher tortuosity in comparison to MSSQ, and tortuosity contributes also to lose energy. It appears that inorganic-based porous structures (pore diameter > 3 nm) with high tortuosity and high OH groups would be good candidates for the production of Ps with low energy. More systematic investigations are necessary to get a clear understanding of the most effective features of the pores to Ps production.

4.2 Ps formation and cooling in SiO_2 for antimatter experiments

For their high Ps yield, high diffusivity and low pick-off rate porous silica appear to be the best candidates for Ps formation, cooling and emission into a vacuum. In the following we discuss the silica-based materials investigated by various research groups with the purpose to get *o*-Ps for antimatter production.

The Trento group (Italy) produced promising materials for *o*-Ps production[26,32] by using mesoporous silicon chips. The mesopores were formed by electrochemical etching of a Si p-type (100) substrate in hydrofluoric acid (HF) solutions. The resulting chips featured an array of straight parallel mesopores (perpendicular to the surface) of a few microns length and with tunable mesopores size in the range 5–20 nm. Various porous silicon samples were prepared in order to investigate the dependence of *o*-Ps production on the mesopore size and the

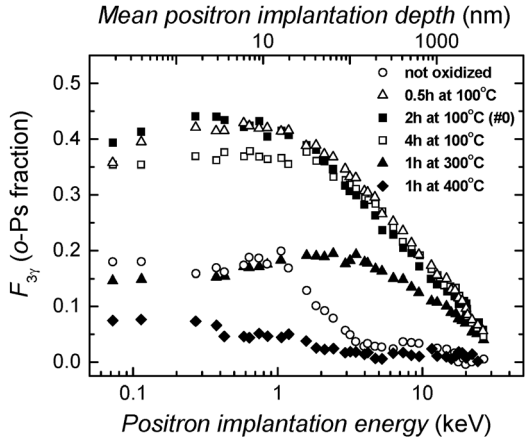

Fig. 6 Fraction of implanted positrons annihilating as *o*-Ps as a function of positron implantation energy (lower scale) and mean positron implantation depth (upper scale). Samples with nanochannels: not oxidized, oxidized at different times and different temperatures (Reprinted figure with permission from ref. 32. Copyright (2010) by the American Physical Society. DOI: 10.1103/PhysRevB.81.235418).

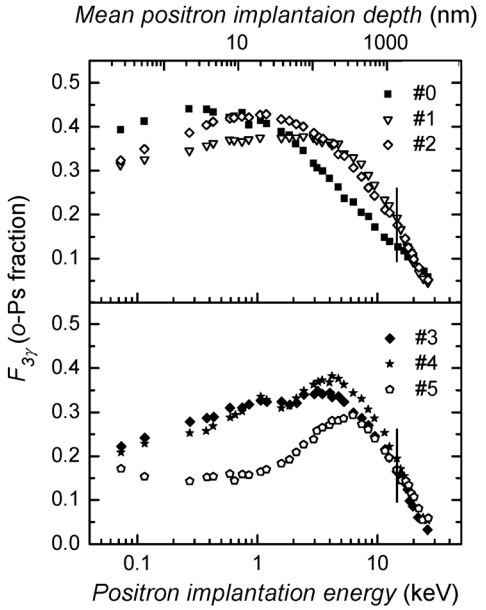

Fig. 7 Fraction of implanted positrons annihilating as Ps as a function of positron implantation energy (lower scale) and mean positron implantation depth (upper scale). The vertical lines mark the border between the silicon region with nanochannels and the bulk silicon (Reprinted figure with permission from ref. 32. Copyright (2010) by the American Physical Society. DOI: 10.1103/PhysRevB.81.235418).

surface chemistry of the porous silicon. The first mesoporous silicon chip was immediately transferred in a ultra high vacuum chamber to prevent any oxidation of the mesopores walls; the surface groups being almost only Si–H functions. The other mesoporous silicon samples were oxidized in air at various temperatures between 373 and 673 K for different times; the surface groups being Si–H, Si–OH and Si–O–Si functions. The fraction of implanted positrons annihilating as *o*-Ps was measured by means of the 3γ method through the $F_{3\gamma}$ parameter (Section 3). The first sample (almost Si–H surface groups) allowed the authors to obtain a high and stable *o*-Ps yield, if the sample was kept under vacuum. However, *o*-Ps yield was rapidly reduced when the sample was exposed to air. Concerning the oxidized samples, the highest *o*-Ps yield was obtained after thermal treatment at 373 K for 2 hours, as can be seen in Fig. 6. On the basis of these results, a series of 6 samples was prepared using these values of temperature and time, but subjected to a different number of etchings in HF solution for 1 min and subsequent re-oxidation in air for 2 hours at 373 K, in order to increase the diameter of the pores without changing their surface chemistry.

Fig. 7 shows the $F_{3\gamma}$ curves obtained by measuring the samples labelled #0, #1, #2, #3, #4, and #5, where the number indicates the number of supplementary etching cycles (and oxidation) in comparison to the first sample 0. Adding etching cycles progressively increased the diameter of the pores: 4–7 nm (sample 0), 8–12 nm (sample 1), 8–14 nm (sample 2), 10–16 nm (sample 3), 14–20 nm (sample 4) and 80–120 nm (sample 5). The highest Ps yield, around 45% of the implanted positrons with a kinetic energy of 1 keV, was found for the samples characterized by diameters in the range 4–7 nm and 8–12 nm. Optimum pore size for maximum Ps production in mesoporous silicon should be around 8 $\pm$ 4 nm for straight pores (with low pore tortuosity) with a right proportion of Si–H and Si–OH groups at the surface (which remains to be precisely defined by other techniques as FTIR), or in other words with a right proportion of hydrophobic and hydrophilic groups on the surface. It is worth mention that porous silicon after partial or complete oxidation is used as a sensor for liquid and gases since it is hydrophilic.[33]

Ordered mesoporous silica (MCM-41 and SBA-16 type) thin films obtained by spin coating on glass have been analyzed for *o*-Ps production for antihydrogen generation by Crivelli *et al.*[34] MCM-41 and SBA-16 continuous, defect-free, thin films were prepared using tetraethoxysilane (TEOS) and cetyltrimethyl ammonium chloride (CTAC)[35] and Pluronic F127 triblock copolymer ($EO_{106}PO_{70}EO_{106}$),[36,37] respectively. After calcination MCM-41 thin film features a homogeneous pore size around 3 nm and SBA-16 an ordered structure of interconnected cavities of 5 nm size and 4 nm windows. By using the Ps-TOF spectroscopy the authors find that *o*-Ps yield is almost independent of the temperature in which the sample was put between 50 and 400 K, showing the stability of the porous structure and of their surface chemistry in this range of temperature. The slight variation could come from the fact that the *o*-Ps escape probability into vacuum decreases when the temperature decreases. Concerning the average energy of the *o*-Ps emitted in a vacuum, the sample with smaller mesopores (MCM-41 type) shows a higher energy (73 meV) in comparison to the sample with larger, less homogeneous pores (SBA-16 type) inducing an energy of 45 meV as expected for smaller pores materials by considering the Heisenberg principle. It is found that pore diameter of SBA-16 is 1.3 times higher than MCM-41, according to the adopted model to estimate the pore sizes,[34] which corresponds to the opening of the windows in SBA-16 materials. Ordered mesoporous

Table 1 Lifetimes and intensities resulting from the time annihilation spectra of aerogel and MCM-41

Sample	τ_1 (ns)	I_1 (%)	τ_2 (ns)	I_2 (%)	τ_3 (ns)	R_3 (nm)	I_3 (%)	τ_4 (ns)	R_4 (nm)	I_4 (%)
Aerogel	0.25(3)	43(3)	0.60(3)	28(3)	3.5(3)	0.40(1)	0.8(1)	128(4)	15(1)	28.2(9)
MCM-41	0.22(3)	48(3)	0.60(3)	34(3)	3.1(2)	0.37(1)	3.9(4)	106(4)	5.8(5)	13.3(6)

silica materials as MCM-41 with their homogeneous straight mesopores appear therefore to be good candidates to explore Ps production.

Very recently we deeply studied another type of MCM-41 material, a powder of swelled-MCM-41 type material (11 nm pore diameter) in pellets form to generate *o*-Ps and compared it to a hydrophobic silica aerogel of very high porosity.

The silica aerogel sample was prepared by a two-step polymerization process where a first silica sol is formed from tetramethoxysilane in acidic media, followed by alcohol removal,[38] then acetonitrile is added to inhibit the gelation, and then water, methyltriethoxysilane and ammonium hydroxide are added.[39] The resulting gel is directly dried by supercritical extraction of the solvent (acetonitrile) in an autoclave at 568 K and 5.4 MPa to maintain the highly expanded state form of aerogel in the form of a three dimensional array of filaments and to give the hydrophobic character to the aerogel with the methyl groups. The aerogel samples had a density of 85 mg cm^{-3} and a porosity of about 96%, a pore diameter around 25 nm (as measured by the Broekhoff and De Boer method[40]), a surface area of 660 m^2 g^{-1} and a pore volume of 2.5 mL g^{-1}. The swelled-MCM-41[41–44] sample was prepared in an autoclave at 388 K by using cetyltrimethylammonium bromide (CTAB), 1,3,5-trimethylbenzene (TMB) as a swelling agent, pyrogenic silica (Aerosil 200 Degussa), sodium hydroxide, and deionized water in molar ratios 1 SiO_2 : 0.26 NaOH : 0.035 $NaAlO_2$: 0.1 CTAB : 20 H_2O : 1.3 TMB. The resulting material was calcined in air at 773 K for 8 h to liberate the porosity and then was compressed to form a pellet. The density of the swelled-MCM-41 sample was 390 mg cm^{-3} with a mesoporous volume of 1.65 cm^3 g^{-1}. The mesopore diameter of the swelled-MCM-41 was about 11 nm (as measured by the Broekhoff and De Boer method[40]) and the surface area was 900 m^2 g^{-1}.

Thickness of MCM-41 and aerogel samples (about 1 and 1.5 cm, respectively) was sufficient to perform a positron annihilation lifetime study. In the case of MCM-41 the positron source was inserted between the sample and a tungsten sheet, where Ps is not formed, in order to annihilate all the emitted positrons. Indeed, the goal was to determine the *o*-Ps lifetimes. The samples were inserted into a glass vial and evacuated by a turbo pump. For each sample three measurements were carried out; spectra were analyzed in four components. The results are shown in Table 1. The two shortest lifetime components are ascribed to free positrons which annihilate in the bulk SiO_2 (and in tungsten in the case of MCM-41 sample) and in defects as well as to *p*-Ps, whose component, having faint intensity, cannot be distinguished from the others. The lifetime of the third component (a few ns) probably comes from *o*-Ps annihilating in structural defects, analogously to the free volume formed in the amorphous phase of polymers. Also the value of the lifetime is quite similar to that found in polymers.[5] The fourth component is the most interesting one, since it can be attributed to *o*-Ps annihilations in the mesopores. Intensity of the fourth component in the case of the MCM-41 is not significant due to the presence of the tungsten layer in the experimental configuration. More interestingly, it is possible to relate the lifetime to the sizes of the pore through a quantum mechanical model originally proposed by Tao[45] and further worked out by Eldrup *et al.*[46] By assuming a pore as a spherical void, they determined the following relationship between the *o*-Ps pick-off decay rate $\lambda_{p.o.}$ (ns^{-1}) and the pore radius R:

$$\lambda_{p.o.} = \lambda_0 \left[\frac{\Delta R}{R + \Delta R} + \frac{1}{2\pi} \sin\left(2\pi \frac{R}{R + \Delta R} \right) \right] \qquad (7)$$

where ΔR (0.17 nm) describes the penetration of *o*-Ps wave function into the bulk and $\lambda_0 = 2$ ns^{-1} is the annihilation rate of *o*-Ps in the presence of a high electron density. A similar formula can be obtained by assuming a cylindrical geometry for the pore.[47,48] Anyway, sizes obtained by different geometries are quite similar.[49] By inverting eqn (7) or analogous it is possible to get the radius of the pore. A more complicated formula (the so-called extended Tao–Eldrup model)[50,51] is necessary in the case of lifetimes of the order of 100 ns or more, as in aerogel and MCM-41 samples, to take into account possible excited states in the trap. The radii shown in Table 1, near the corresponding lifetimes, were obtained by using the Tao–Eldrup model in spherical geometry (eqn (7)) for the third component, or the extended Tao–Eldrup model in cylindrical geometry for the fourth component. The results of the *o*-Ps lifetimes in the investigated samples indicate that average radii are about 6 nm and 15 nm in MCM-41 and aerogel, respectively, in accordance with nitrogen sorption measurements. These dimensions are in the range of optimum values for *o*-Ps thermalization.[26]

Investigation of *o*-Ps formed in the pores near the surface of MCM-41 and aerogel was carried out by sending a beam of monoenergetic positrons on each sample; positron implantation energy was variable between 1 and 18 keV. Measurements were carried out in a temperature range between 8 and 293 K, under a vacuum level below 10^{-8} mbar, by using a Ge spectrometer to obtain the *o*-Ps fraction formed $f_{3\gamma}$ by means of the 3γ method (Section 3). Fig. 8 shows that the *o*-Ps yield does not depend on temperature for any implantation energies. In Fig. 9 $f_{3\gamma}$ for positrons implanted at 3 keV in both samples as a function of the temperature confirms the stability of these samples in a wide range of temperature[52,53] as previously mentioned by Crivelli *et al.*[34] for ordered mesoporous silica films. Sferlazzo *et al.*[54] identify in crystalline SiO_2 that the physisorbed *o*-Ps emitted from the surface depends on temperature; on the other hand, *o*-Ps produced into the SiO_2 bulk

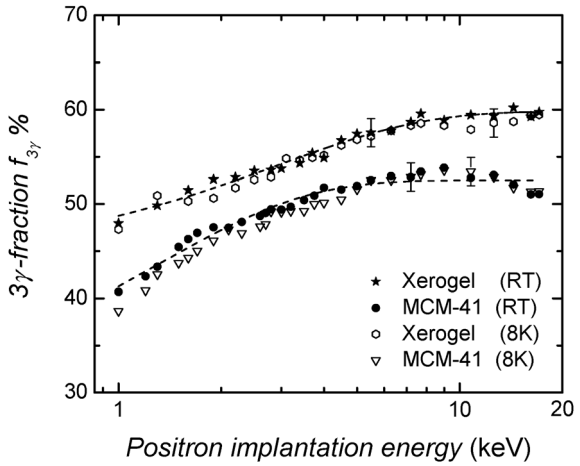

Fig. 8 Positronium fraction $f_{3\gamma}$ as a function of the positron implantation energy in aerogel and MCM-41 measured at room temperature and at 8 K. The dashed lines are only a visual guide. Error bars are shown for one point only in each evolution.

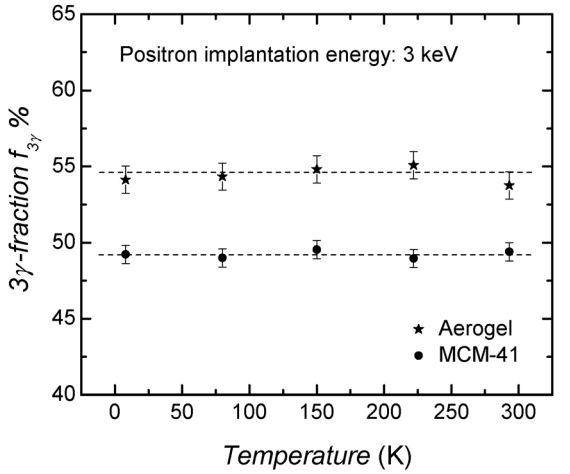

Fig. 9 Ps fraction $f_{3\gamma}$ as a function of the temperature for positron implanted inside the sample at 3 keV in aerogel and swollen MCM-41 samples (reprinted figure with permission from ref. 52. Copyright (2011) by IOP Publishing Ltd. DOI: 10-1088/1742-6596/262/1/012020).

and diffusing to the surface is independent of the temperature. Therefore, the independence from the temperature observed for MCM-41 and aerogel indicate that *o*-Ps would be produced only into the bulk and then diffuses to the porous surface. The produced *o*-Ps thermalizes by means of thousands of collisions with the walls of the pores according to the high survival time (τ_4, Table 1). The decrease of $f_{3\gamma}$ observed at low energy in Fig. 8 is due to the *o*-Ps emission into the vacuum, which implies a decrease of the *o*-Ps detection efficiency. *o*-Ps yield is remarkably high at high implantation energies in comparison to the thin mesoporous films that have been previously presented,[32,34] where it is possible to obtain high yields only at low energies. High yield at high implantation energies requires rather thick samples (tens of microns), a condition easily met with homogenous aerogels and MCM-41 pellets. The maximum positronium fraction $f_{3\gamma}$ in Fig. 8 is about 53% in MCM-41 and about 60% in aerogel.

These results are very promising for the further work, which will be performed on these materials in the AEgIS experiment at very low temperatures, around 0.1 K. A negative effect of a cryogenic environment for a porous substance is the adsorption of residual gases, mainly water vapor and nitrogen,[24,55] and in consequence the formation of ice at the surface of the pores, which hampers the Ps to escape into vacuum. Water absorption by SiO_2 at temperatures below 150 K was ascertained even under ultra-high vacuum conditions.[53] Baking the vacuum chamber at high temperatures ($\sim$473 K), which would solve the problem, is not possible in antihydrogen experiments due to the presence in the chamber of electronics and detectors. Water adsorption could be prevented with the introduction of hydrophobic patches into the surface of mesoporous SiO_2 structure. Aerogel and swelled-MCM-41 possess intrinsically hydrophobic patches on their porous structure with methyl groups for aerogel and with siloxane groups at the surface of the pore of swelled-MCM-41 as demonstrated elsewhere.[56] The first results performed at very low temperature (8 K) for aerogel and MCM-41 (Fig. 9), indicate that the effect of gas adsorption or condensation at low temperature does not influence the *o*-Ps yield for these materials.

When the porosity is very high and the pores are interconnected, *o*-Ps diffuses during cooling. In order to obtain the positronium diffusion length L_{Ps} the mesoporous samples were capped by an Al film having a thickness of about 110–120 nm, to prevent *o*-Ps escape into vacuum. The results are shown in Fig. 10 for MCM-41 and aerogel samples. Ps formation is almost zero for implantation energies of about 2 keV; indeed, all the incident positrons annihilate in the metallic layer where no Ps formation is expected. At lower energies ($<$1.5 keV) a fraction of the positrons form Ps at the Al surface. The results of the positronium fraction as a function of the positron incident energy obtained in a capped porous sample were analyzed by means of a semi-linear fitting procedure using the VEPFIT program.[57] This program extracts relevant parameters from positron measurements on layered structures. In the present case our attention is focused on the Ps diffusion length.

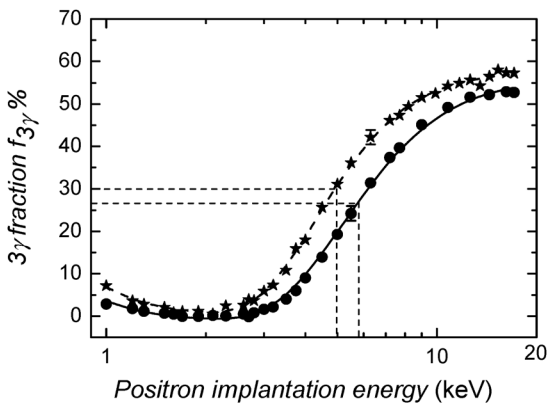

Fig. 10 Ps fraction $f_{3\gamma}$ as a function of the positron implantation energy in aerogel (stars) and MCM-41 (circles) measured at room temperature. The samples were capped with Al to avoid the Ps escape. Estimated positronium mean diffusion length is 2.3 and 1.0 μm in aerogel and MCM-41, respectively. Error bars are shown for one point only in each evolution.

Table 2 Ps diffusion length in aerogel and MCM-41 samples obtained by means of the Vepfit model. The thicknesses Z of the Al capping layer and the interface between Al and the porous materials are also included. The value indicated with F is a fixed parameter

	Z_{Al} (nm)	Z_{int} (nm)	L_{Ps} (nm)
Aerogel	108 ± 6	15F	2300 ± 300
MCM-41	120 ± 5	8F	960 ± 50

The experimental data were fitted using a model of layers comprised of: a surface, an aluminium layer, an interface and a semi-infinite layer of the mesoporous material. The transport of positrons after implantation and thermalization in a solid is approximated by the diffusion theory. According to the fitting of the results the positron diffusion length after thermalization is much lower than the Ps diffusion length. Indeed, the positron diffusion length in the studied materials is about 10 nm and the *o*-Ps diffusion length, as it will be seen, is of the order of 10^3 nm. Under this condition it is possible to assume that the diffusion equation holds only for Ps. The positrons implanted at the interface do not influence the calculated profiles.

The capping layer of Al was deposited by molecular beam epitaxy. The interface between Al and the porous material used in the analysis model takes into account a possible contamination effect of few nanometres on the porous material with Al during evaporation.

The continuous and dashed lines in Fig. 10 correspond to the best fit values of the *o*-Ps diffusion length. The most relevant parameters of the fitting procedure are shown in Table 2.

The adopted model is based on the assumption that the diffusion coefficient does not depend on the *o*-Ps temperature during its cooling. Thus, the diffusion coefficients D_{Ps} ($D_{Ps} = {L_{Ps}}^2/\tau$, calculated using the fourth lifetime *o*-Ps component, see Table 1) are: 0.41(9) $cm^2\ s^{-1}$ and 0.087(9) $cm^2\ s^{-1}$, respectively, in aerogel and MCM-41. The values found for the diffusion length, which are rather high, are consistent with the high *o*-Ps emission from the material, even for high positron implantation energies.

The vertical dashed lines in Fig. 10 represent important indirect information. These lines correspond to the positron implantation energies for which 50% of the *o*-Ps formed takes contact with the Al capping layer and is quenched by pick-off annihilating in two gamma rays. The implantation energies are about 5 and 6 keV in aerogel and MCM-41, respectively. To obtain an estimation of the mean implantation depth $z_{1/2}$ for which 50% of the *o*-Ps formed escapes into the vacuum in a sample without the Al capping layer, it is necessary to subtract to the obtained energies, the implantation energy to overcome the Al foil. This estimation says that $z_{1/2}$ is about a half of the *o*-Ps diffusion length for each material ($z_{1/2} \approx 1/2\ L_{Ps}$), corresponding to positrons implanted at ~1.8 and ~2.6 keV in aerogel and MCM-41, respectively. It is clear that a balance must be reached between efficient *o*-Ps thermalization necessary for AEgIS, which requires deep positron implantation, and high *o*-Ps yield under vacuum, which is favoured by implantation depths not large in comparison with the *o*-Ps diffusion length. The necessary positron implantation energy to obtain thermalized positronium in open porous silica is typically of the order of 10^4 eV and allows one to obtain a few percent of the *o*-Ps formed outside the target.[26,28] The results obtained in MCM-41 and aerogel indicate that these materials are potentially good converters for the AEgIS experiment under the following aspects: high *o*-Ps yield, independently on temperature and on the effect of gas adsorption at low temperature, long survival time of *o*-Ps inside the pores and very high *o*-Ps mobility. Indeed, the literature tells that in these families of homogeneous porous materials Ps thermalization and escape into vacuum were ascertained.[18,19,58] In particular, Mills *et al.*[28] have observed 2% and 8% of Ps thermalized (with respect to the implanted positrons) into the vacuum at 4.2 and 77 K, respectively, in an homogeneous porous silica with a mass density (180 mg cm^{-3}) intermediate between the studied aerogel and MCM-41.

5. Conclusions

Each component plays an important role in the complex experiment designed to measure gravitational effects on antihydrogen; nevertheless, a prominent part will be done by Ps. A high yield of such an atom with sufficiently low kinetic energy (''cold'' *o*-Ps) will make possible to obtain a sufficient amount of antihydrogen to carry out the gravitational experiment with the necessary precision. Therefore, the correct behaviour of the converter on which positrons will be implanted is of the utmost importance. According to the above discussion the converter will necessarily be a porous material; the trend of the various research groups is towards mesoporous silica based materials with a partially hydrophobic surface.

An efficient *o*-Ps cooling requires high positron implantation energies, in order to increase the pattern of *o*-Ps formed in the pore. This implies a thickness of several microns for samples having low density, a condition easily met in porous materials. On the other hand, a longer *o*-Ps path increases the number of collisions between *o*-Ps and pore walls, which increases the annihilation probability by pick-off: this decreases the *o*-Ps fraction emitted by the target. Therefore, a compromise between cooling and *o*-Ps yield is required, which must be searched for as a function of the investigated material.

Measurements of *o*-Ps yield in porous materials must face also various experimental difficulties, among them is the possible adsorption of residual gases at the porous surface at low temperature. These gases are still present at ultra high vacuum levels and play an important influence at low temperature due to the sticking coefficient, near to 1.[55,59] Furthermore, a subject yet to be explored is the durability of a porous medium to a prolonged irradiation by the positrons as well as by the γ-rays emitted during the annihilation process. Indeed, a high radiation dose is responsible for the formation of paramagnetic centres in SiO_2,[60] which decreases *o*-Ps formation.

In conclusion, only further tests, in particular at temperatures comparable to those of the real experiment, can determine which material, among those investigated until now,

will be able to assure not only the best performances but also their constancy with time. Hydrophobic MCM-41 and aerogels are very promising materials.

Notes and references

1 *PET: physics, instrumentation and scanners*, ed. M. E. Phelps, Springer, New York, 2006.
2 N. Bassler, *et al.*, *Radiother. Oncol.*, 2008, **86**, 14.
3 A. Somoza, A. Dupasquier and R. Ferragut, *Phys. Status Solidi c*, 2009, **6**, 2295.
4 R. Krause-Rehberg and H. S. Leipner, *Positron Annihilation in Semiconductors, Solid-State Sciences*, Springer, Berlin, 1999, vol. 127.
5 G. Dlubek, in *Polymer Physics: from Suspensions to Nanocomposites and beyond*, ed. L. Utracki and A. Jamieson, John Wiley & Sons, Inc., New York, 2010, ch. 11.
6 E. V. Canesi, *et al.*, *Energy Environ. Sci.*, 2012, **5**, 9068.
7 D. W. Gidley, H. G. Peng and R. S. Vallery, *Annu. Rev. Mater. Res.*, 2006, **36**, 49.
8 A. Di Piazza, C. Müller, K. Z. Hatsagortsyan and C. H. Keitel, *Rev. Mod. Phys.*, 2012, **84**, 1177.
9 A. P. Mills Jr, *Radiat. Phys. Chem.*, 2007, **76**, 76.
10 D. S. Hajdukovic, *Astrophys. Space Sci.*, 2011, **334**, 215.
11 G. J. Ni, in *Relativity, Gravitation, Cosmology*, ed. V. V. Dvoeglazov and A. A. Espinoza Garrido, Nova Science Publications, 2004, p. 123.
12 A. G. Riess, *et al.*, *Astron. J.*, 1998, **116**, 1009.
13 A. Kellerbauer, *et al.* (AEgIS collaboration), *Nucl. Instrum. Methods Phys. Res., Sect. B*, 2008, **266**, 351.
14 R. Ferragut, A. Calloni, A. Dupasquier, G. Consolati, F. Quasso, M. G. Giammarchi, D. Trezzi, W. Egger, L. Ravelli, M. P. Petkov, S. M. Jones, B. Wang, O. M. Yaghi, B. Jasinska, N. Chiodini and A. Paleari, *J. Phys.: Conf. Ser.*, 2010, **225**, 012007.
15 A. P. Mills Jr, in *Physics with many positrons*, ed. A. Dupasquier, A. P. Mills Jr and R. S. Brusa, IOS Press, Amsterdam, 2010.
16 T. J. Murphy and C. M. Surko, *Phys. Rev. A: At., Mol., Opt. Phys.*, 1992, **46**, 5696.
17 Y. Nagashima, Y. Morinaka, T. Kurihara, Y. Nagai, T. Hyodo, T. Shidara and K. Nakahara, *Phys. Rev. B: Condens. Matter Mater. Phys.*, 1998, **58**, 12676.
18 H. K. M. Tanaka, T. Kurihara and A. P. Mills Jr, *J. Phys.: Condens. Matter*, 2006, **18**, 8581.
19 A. P. Mills Jr, *Phys. Rev. Lett.*, 1978, **41**, 1828.
20 J. Lahtinen, A. Vehanen, H. Huomo, J. Makinen, P. I-Iuttunen, K. Rytsolii, M. Bentzon and P. Hautojarvi, *Nucl. Instrum. Methods Phys. Res., Sect. B*, 1986, **17**, 73.
21 D. M. Schrader and Y. C. Jean, in *Positron and Positronium Chemistry*, ed. D. M. Schrader and Y. C. Jean, Elsevier, Amsterdam, 1988, ch. 1.
22 G. Consolati, I. Genco, M. Pegoraro and L. Zanderighi, *J. Polym. Sci., Part B: Polym. Phys.*, 1996, **34**, 357.
23 M. P. Petkov, M. H. Weber, K. G. Lynn and K. P. Rodbell, *Appl. Phys. Lett.*, 2001, **79**, 3884.
24 F. Moia, R. Ferragut, A. Dupasquier, M. Giammarchi and G. Q. Ding, *Eur. Phys. J. D*, 2012, **66**, 124.
25 R. S. Brusa and A. Dupasquier, in *Physics with many positrons*, ed. A. Dupasquier, A. P. Mills Jr and R. S. Brusa, IOP, Amsterdam, 2010, pp. 245–296.
26 S. Mariazzi, P. Bettotti and R. S. Brusa, *Phys. Rev. Lett.*, 2010, **104**, 243401.
27 A. P. Mills Jr, E. D. Shaw, M. Leventhal, R. J. Chichester and D. M. Zuckerman, *Phys. Rev. B: Condens. Matter Mater. Phys.*, 1991, **44**, 579.
28 A. P. Mills Jr, E. D. Shaw, R. J. Chichester and D. M. Zuckerman, *Phys. Rev. B: Condens. Matter Mater. Phys.*, 1989, **40**, 2045.
29 Y. Kobayashi, K. Ito, T. Oka and K. Hirata, *Radiat. Phys. Chem.*, 2007, **76**, 224.
30 C. He, *et al.*, *Phys. Rev. B: Condens. Matter Mater. Phys.*, 2007, **75**, 195404.
31 R. S. Yu, T. Ohdaira, R. Suzuki, K. Ito, K. Hirata, K. Sato, Y. Kobayashi and J. Xu, *Appl. Phys. Lett.*, 2003, **83**, 4966.
32 S. Mariazzi, P. Bettotti, S. Larcheri, L. Toniutti and R. S. Brusa, *Phys. Rev. B: Condens. Matter Mater. Phys.*, 2010, **81**, 235418.
33 O. Bisi, L. Ossicini and L. Pavesi, *Surf. Sci. Rep.*, 2000, **38**, 1.
34 P. Crivelli, U. Gendotti, A. Rubbia, L. Liszkay, P. Perez and C. Corbel, *Phys. Rev. A*, 2010, **81**, 052703.
35 Y. Cohen, K. Landskron, N. Tetretault, S. Fournier-Bidoz, B. Hatton and G. A. Ozin, *Adv. Funct. Mater.*, 2005, **15**, 593.
36 D. Zhao, J. Feng, Q. Huo, N. Melosh, G. H. Fredrickson, B. F. Chmelka and G. D. Stucky, *Science*, 1998, **279**, 548.
37 D. Zhao, P. Yang, N. Melosh, J. Feng, B. F. Chmelka and G. D. Stucky, *Adv. Mater.*, 1998, **10**, 1380.
38 T. M. Tillotson and L. W. Hrubesh, *J. Non-Cryst. Solids*, 1992, **145**, 44.
39 D. Brownlee, *et al.*, *Science*, 2006, **314**, 1711.
40 J. C. P. Broekhoff and J. H. De Boer, *J. Catal.*, 1968, **10**, 377.
41 C. T. Kresge, M. E. Leonowicz, W. J. Roth, J. C. Vartuli and J. S. Beck, *Nature*, 1992, **359**, 710.
42 J. S. Beck, *et al.*, *J. Am. Chem. Soc.*, 1992, **114**, 10834.
43 A. Galarneau, D. Desplantier, R. Dutartre and F. Di Renzo, *Microporous Mesoporous Mater.*, 1999, **27**, 297.
44 M. F. Ottaviani, A. Moscatelli, D. Desplantier-Giscard, F. Di Renzo, P. J. Kooyman, B. Alonso and A. Galarneau, *J. Phys. Chem. B*, 2004, **108**, 12123.
45 S. J. Tao, *J. Chem. Phys.*, 1972, **56**, 5499.
46 M. Eldrup, D. Lightbody and N. J. Sherwood, *Chem. Phys.*, 1981, **63**, 51.
47 B. Jasinska, A. E. Koziol and T. Goworek, *J. Radioanal. Nucl. Chem.*, 1996, **210**, 617.
48 G. Consolati, F. Quasso, R. Simha and G. B. Olson, *J. Polym. Sci., Part B: Polym. Phys.*, 2005, **43**, 2225.
49 G. Consolati, *J. Chem. Phys.*, 2002, **117**, 7279.
50 T. Goworek, K. Ciesielski, B. Jasinska and J. Wawryszczuk, *Chem. Phys.*, 1998, **230**, 305.
51 D. W. Gidley, *et al.*, *Phys. Rev. B: Condens. Matter Mater. Phys.*, 1999, **60**, R5157.

52 R. Ferragut, A. Dupasquier, A. Calloni, G. Consolati, F. Quasso, M. P. Petkov, S. M. Jones, A. Galarneau and F. Di Renzo, *J. Phys.: Conf. Ser.*, 2011, **262**, 012020.
53 R. Ferragut, *et al.* (AEgIS collaboration), *Can. J. Phys.*, 2011, **89**, 17.
54 P. Sferlazzo, S. Berko and K. F. Canter, *Phys. Rev. B: Condens. Matter Mater. Phys.*, 1985, **32**, 6067.
55 O. Sneh, M. A. Cameron and S. M. George, *Surf. Sci.*, 1996, **364**, 61.
56 M. F. Ottaviani, A. Galarneau, D. Desplantier-Giscard, F. Di Renzo and F. Fajula, *Microporous Mesoporous Mater.*, 2001, **44–45**, 1; A. Moscatelli, A. Galarneau, F. Di Renzo and F. Ottaviani, *J. Phys. Chem. B*, 2004, **108**, 18580.
57 A. van Veen, H. Schut, J. de Vries, R. A. Hakvoort and M. R. Ijpma, in *Positron Beam for Solids and Surfaces*, AIP Conf. Proc. ed. P. J. Shultz, G. R. Massoumiand and P. J. Simpson, AIP, New York, 1990, vol. 218, p. 171.
58 Y. Nagashima, M. Kakimoto, T. Hyodo, K. Fujiwara, A. Ichimura, T. Chang, J. Deng, T. Akahane, T. Chiba, K. Suzuki, B. T. A. McKee and T. Stewart, *Phys. Rev. A*, 1995, **52**, 258.
59 S. H. M. Deng, D. B. Cassidy, R. G. Greaves and A. P. Mills Jr, *Appl. Surf. Sci.*, 2007, **253**, 9467.
60 H. Saito, Y. Nagashima, T. Hyodo and T. Chang, *Phys. Rev. B: Condens. Matter Mater. Phys.*, 1995, **52**, R689.

